Experimental studies on scour of supercritical flow jets in upstream of screens and modelling scouring dimensions using artificial intelligence to combine multiple models (AIMM)

Sina Sadeghfam, Rasoul Daneshfaraz, Rahman Khatibi and Omar Minaei

ABSTRACT

Performances of screens in watercourses are investigated for dissipating energy of supercritical flows, capable of inducing scour or stabilising hydraulic jumps. Subsequent scouring pits are characterised by pit depth and pit length. Inherent processes are studied through laboratory tests by producing a set of empirical data to formulate a model of the scour for explaining subsequent processes. The experimental set-up comprises: (i) Froude number of supercritical flows (range: 3.5–8.0); (ii) particle densimetric Froude number (range: 2–10) using five granular samples; and (iii) two screen porosities (40% and 50%). Trained and tested artificial intelligence models explain the data by expressing depth and length of the pit through the following levels: Level 1: use the experimental data and test the models of: Sugeno fuzzy logic (SFL) and neuro-fuzzy (NF); and Level 2: use outputs of Level 1 models as inputs to support vector machine (SVM). The results reveal that the Level 2 model improves model performances compared with the single models with respect to R^2, root mean square error (RMSE), Nash–Sutcliffe coefficient (NSC) and residual errors. While Level 1 models remain fit-for-purpose, the comparative improvement from Level 1 to Level 2 can be as high as 58% in terms of NSC for the testing phase.

Key words | multiple models, NF, scour, screen, SFL, SVM

Sina Sadeghfam
Rasoul Daneshfaraz (corresponding author)
Omar Minaei
Department of Civil Engineering,
Faculty of Engineering,
University of Maragheh,
Maragheh, East Azerbaijan,
Iran
E-mail: *daneshfaraz@maragheh.ac.ir*

Rahman Khatibi
GTEV-ReX Limited,
Swindon,
UK

LIST OF SYMBOLS

d_{50} median size of particles
D_s maximum depth of scouring pit
F_0 particle densimetric Froude number
Fr_A Froude number of supercritical flow jets
L_s maximum length of scouring pit
P screen porosity
s relative density of the particles
V_A velocity of entering jet at section A
w gate opening
x longitudinal coordinate
x_s distance between screen location and the sluice gate
y_B flow depth at section B (tailwater)
ρ density of water
ρ_s density of granular particles
σ_g geometric standard deviations of the grains
μ dynamic viscosity of water

INTRODUCTION

Scouring caused by screens under supercritical flows in open channel reaches are investigated, where the reach is a complex of a sluice gate and a screen but with a stilling basin in between them giving rise to a pit as an outcome

doi: 10.2166/hydro.2019.076

of scouring processes. The pit is induced by supercritical flows in the stilling basin over a moveable bed. While studies of hydraulic processes in such reaches go back to 2000 with a focus on flow-energy dissipation, there is no study to predict their scours by modelling or by empirical equations for their estimation. This paper fills the gap by advancing the state-of-the-art by investigating moveable beds through introducing two equations to characterise pit scours in terms of the pit depth and length. The parameters in these empirical equations are identified by a modelling strategy using artificial intelligence (AI) models at two levels.

The use of screens are well-established over time in open channels to ensure the removal of coarse impurities. As energy dissipators, screens are of recent introduction and go back to the study of Rajaratnam & Hurtig (2000). Their study reveals the following: screens cause a higher energy dissipation compared to free hydraulic jump; and screens are effective in stabilising the location of hydraulic jump. Several other subsequent studies investigate the effect of such parameters as the location of screens and porosity (Rajaratnam & Hurtig 2000), location and thickness of screens (Çakır 2003), effects of sloping screens (Bozkuş *et al.* 2005), types of hydraulic jump (Sadeghfam *et al.* 2014) and combining screens with baffle-like structures (Daneshfaraz *et al.* 2017). A summary of various studies on scour pits is presented in Table 1 along with the range of their main parameters, e.g., Froude number. Their salient findings demonstrate that energy dissipation of a screen with 40% porosity is more efficient than the screen with 50% porosity (Rajaratnam & Hurtig 2000; Çakır 2003; Sadeghfam *et al.* 2014); thickness of individual screens does not significantly affect dissipation but double screens perform better than single screens (Çakır 2003). Nonetheless, the paper employs a single screen dissipating energy over an experimental stilling basin through a channel with movable bed of variable Froude number and using different screen porosities.

Several studies focus on scouring at the downstream of hydraulic structures, which may be divided into two groups: scouring induced by subcritical flows and those by supercritical flows. Scouring by subcritical flows have focused on the downstream of structures like bridge piers, drops, bridge abutment and submarine pipeline (e.g., Roushangar *et al.* 2016). In these structures, the contact of flow with the body of the structure creates eddy currents, which encourage local scouring. Studies cited above developed equations to describe scouring variations as a function of such parameters as median diameter of grains

Table 1 | Specifications of experiments conducted by other researchers along with the present study

Researcher(s)	Supercritical Froude number range	Porosity (%)	Arrangement	Other specification	Fixed bed	Movable bed	Model types		
							Experimental	Numerical	AI
Rajaratnam & Hurtig (2000)	5–13; 4–7.2	40–50	Single, Double; Triangle	Screens material: plastic; square-shaped openings	✓		✓		
Çakır (2003)	5–18	20–40; 50–60	Single; Double	Screen thickness 2 and 4 cm	✓		✓		
Bozkuş *et al.* (2004); Bozkuş *et al.* (2007)	5–18	20–60	Single; Double	Screens location up to 100× undisturbed upstream depth	✓		✓		
Bozkuş *et al.* (2005); Bozkuş *et al.* (2006)	5–24	40	Single; Double	Screen inclined: 60°, 75°, and 90° with respect to horizontal	✓		✓		
Bozkuş & Aslankara (2008)	5–22.5	40	Multiple screens	–	✓		✓		
Sadeghfam *et al.* (2014)	2.5–8.5	40–50	Single; Double	Submerged hydraulic jump	✓		✓		
Daneshfaraz *et al.* (2017)	2–10	40–50	Single	Used baffles in stilling basin	✓			✓	
Present study	3.8–7.5	40–50	Single	Scouring in stilling basin		✓	✓		✓

along with grading properties and relative density of grains. Scouring induced by supercritical flows is investigated in structures like stilling basins, cross-vanes and various jets (e.g., Castillo & Carrillo 2017), which develop equations to describe scouring as functions of flow velocity, size of bed materials and relative density.

Locations of hydraulic jumps are at the reach between the sluice gate and the screen, where energy dissipation takes place in the form of breaking eddies and turbulence. If the design is not adequate, excessive scouring cannot be ruled out, as a result of which the stilling basins can be destabilised and thereby threaten the stability of the screen and even that of structures in its upstream and downstream. The subsequent scouring depends on the condition of flow and properties of the bed. The novel features of the present study are the use of a movable bed and modelling the scouring induced by supercritical jet flows.

Literature review also shows the use of artificial intelligence (AI) models to estimate different hydraulic parameters in the fixed bed flumes. These include: energy dissipation over channels with rough-bed by using support vector machine (SVM) (Roushangar & Ghasempour 2019), which is often referred to as a machine learning technique; prediction of discharge coefficient of side weir by using genetic programming (GP) (Uyumaz *et al.* 2014); estimating length of hydraulic jumps in U-shaped channel by using artificial neural networks (ANN) (Houichi *et al.* 2013). Roushangar *et al.* (2019) used ANN and gene expression programming (GEP) for estimating submerged discharge capacity of converging ogee spillways and showed that ANN and GEP provide more accurate results than four conventional relationships. AI models are also used to estimate scouring dimensions in movable bed flumes. Toth & Brandimarte (2011) and Choi *et al.* (2015) used ANN to estimate scour around bridge piers. Sahraei *et al.* (2018) used support vector regression and particle swarm optimisation to estimate load transport rate for bed material. This group of studies report improved prediction accuracies by AI models than by empirical equations.

There are two broad approaches for the application of AI techniques: (i) investigating an innovatory model by comparing its performances with a number of more traditional models; and (ii) using an AI model to combine or run multiple models (AIMM) for more improved accuracies in various water-environmental problems, and this is a program of research on stream flows or groundwater vulnerability studies (Nadiri *et al.* 2017, 2018a, 2018b). This paper uses AIMM and implements it at two levels similar to Nadiri *et al.* (2018a). The following strategy is investigated: (i) at Level 1, two AI models are selected and used for making predictions based on measured data; and (ii) at Level 2, another AI model is used, which combines the Level 1 models. The Level 1 models comprise Sugeno fuzzy logic (SFL) and neuro-fuzzy (NF) and at Level 2 the paper uses SVM to combine the Level 1 models. The SFL, NF and SVM are well-established techniques and therefore the paper suffices to specify them.

The study presented in the paper builds on existing literature but additionally focuses on stilling basins' stability for movable beds. The paper presents new experimental results by considering five types of gravel materials with various gradings towards the main aim of bed stabilisation by coarse granular material in the stilling basin. The effects of flows with different parameters are also considered in terms of such parameters as particle densimetric Froude number over dimensions of scouring pit of stilling basin and standard deviation of particle, where densimetric Froude number is often regarded as a better parameter to study critical flow conditions for the initiation of particle motions. Changes in depth and length of scouring pit are explained and described by the AIMM strategy based on using AI models at two levels.

METHODOLOGY

Experimental set-up and method of experiments

The experiments were conducted in a Plexiglas flume, in which sidewalls and floor dimensions comprised: 5 m length, 0.3 m width and 0.45 m height. Supercritical flow conditions were generated by a steel sluice gate of a plate of 5 mm thick and a gate opening of 13 mm. Screens with 40% porosity (P40) and 50% porosity (P50) were installed at 1 m distance from the gate. Screens were 10 mm thick and their form was circular and 10 mm in diameter. The schematic form of the flume and its set-up are illustrated in Figure 1.

The bed of the stilling basin (the distance between the screen and sluice gate) was filled with granular material of

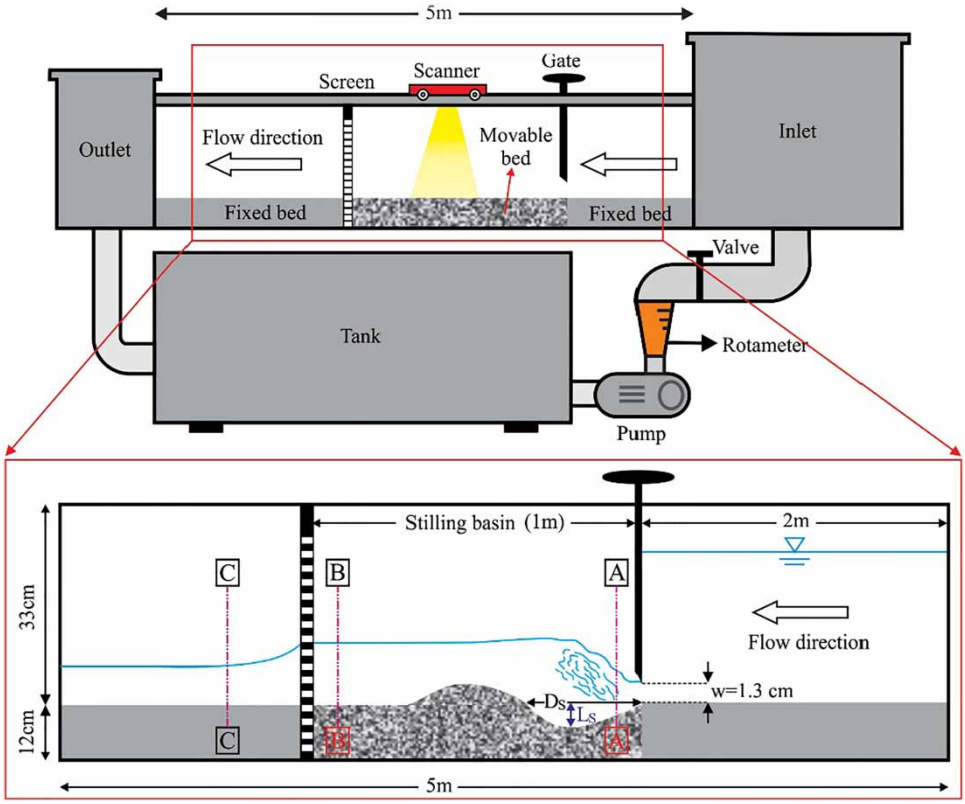

Figure 1 | Overall schematic of the experiment and specifications of the equipment used in the experiments.

different gradings. The fixed bed condition was created using polyethylene plates with 120 mm height and were installed 2 m from the upstream and 2 m from the downstream of the screen. The length of the movable bed was considered 1 m due to the distance from the screen to the gate and its thickness was 120 mm due to the limitation of flow discharge and the height of the channel. The scouring profiles were measured via a laser scanner set (DT50 Laser Class 1) with a precision of 1 mm (Figure 1). The size of the cohesionless grains in the movable bed was selected by a trial-and-error approach. The minimum size of the grains was selected such that the scour depth did not reach the flume bed under the maximum discharge conditions; whereas the maximum size of the grains was selected to create no scouring in maximum discharge conditions.

The role of granular material was investigated by selecting five material samples all with the density of 2,400 kg/m^3 and various diameters. The median diameters of the materials for Samples 1 to 5 were 4.14, 6.76, 10.93, 15 and 24 mm, respectively. Besides, geometric standard deviations of the grains ($\sigma_g = \sqrt{d_{84}/d_{16}}$) for Samples 1 to 5 were calculated to be 1.56, 1.28, 1.22, 1.17 and 1.26, respectively. Notably, d_{84} and d_{16} were the diameters at which 84% and 16% of the mass of the sample comprised particles with a diameter less than these values. The granular composition of the bed material for Samples 1 to 5 are illustrated in Figure 2 in terms of their grading curves.

The continuous supply of the flowing water was facilitated by a pump of the capacity of 450 litres per minute (LPM) and the discharge in the experiments ranged from 150 to 300 LPM. Their Froude numbers ranged from 3.5 to 8 at below the sluice gate (*vena contracta*) for the gate opening of 13 mm. Although the range of Froude number seems limited, it is within the Froude number range of USBR IV stilling basin and the use of screen under higher Froude numbers is unlikely to be practical. Discharge was adjusted through a control valve and was measured via a rotameter.

Considering the time needed for reaching a balanced condition within the scouring pit, the duration of the

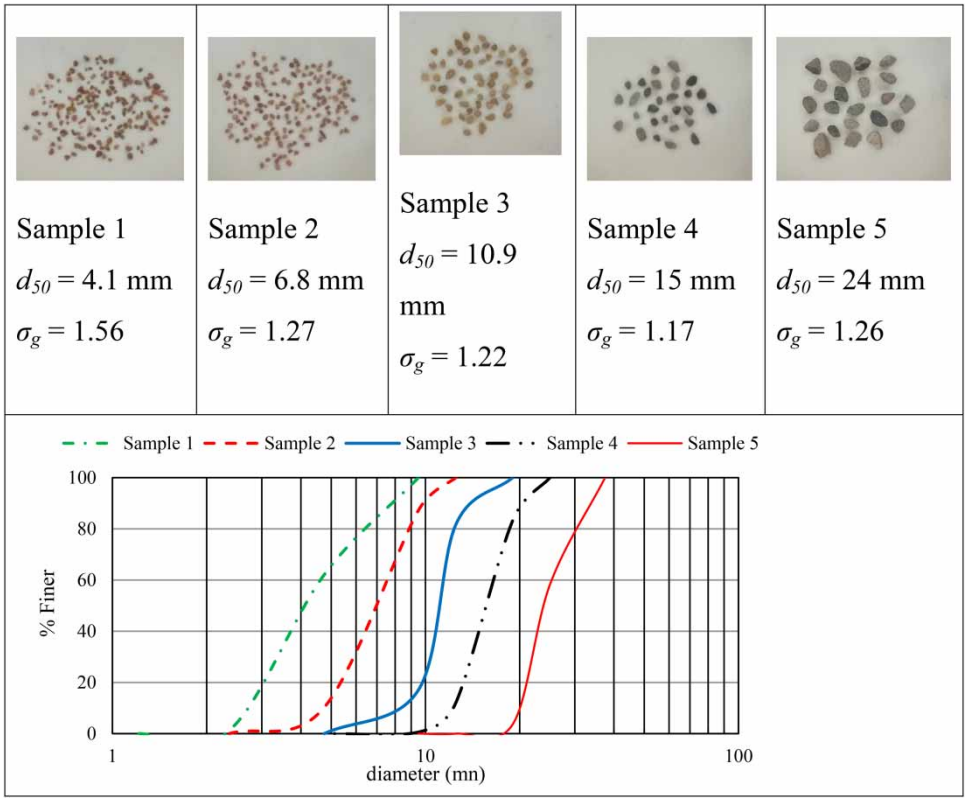

Figure 2 | Grading curve; sample beds used in the experiment and their specifications.

experiment was decided to be 45 minutes so that after this time, the scouring reaches a steady state with no further changes in the dimensions of the pit or after which the experiment continued through repetitive cycles, as discussed later.

Dimensional analysis

The Buckingham-π theorem is used to formulate a mathematical model to the problem of screens of porous plates dissipating scouring. The empirical model comprises a set of two equations to express depth and length of the scoured stilling basin through the following dimensionless parameters with likely effects on scours, as follows:

$$D_s = F_1(V_A, \rho, \rho_s, \mu, g, d_{50}, w, \sigma_g, y_B, P) \quad (1)$$

$$L_s = F_2(V_A, \rho, \rho_s, \mu, g, d_{50}, w, \sigma_g, y_B, P) \quad (2)$$

where D_s and L_s are maximum depth and length of scouring, respectively, V_A is the velocity of entering jet, ρ and ρ_s are the density of water and granular particles, respectively, w is the gate opening, g is the acceleration of gravity, μ is the dynamic viscosity of water, d_{50} is the median size of particles, y_B is the tailwater and σ_g is the standard deviation of particles, P is screen porosity. Notably, some parameters such as screen location and arrangement are not considered in this study but can be investigated in future research. The choice of variables in dimensional analysis depends on the nature of the problem and expert judgement. This study considers the following contributions: fluid defined in terms of: ρ, μ, mobile bed defined in terms of: ρ_s, d_{50}, σ_g; screen defined in terms of: y_B, P; and hydraulics defined in terms of: V_A, w. Using the Buckingham π-theorem, consider dimensionless parameters in terms of the following equations:

$$\frac{D_s}{w} = F_3\left(\frac{y_B}{W}, F_0, \sigma_g, P\right) \quad (3)$$

$$\frac{L_s}{w} = F_4\left(\frac{y_B}{W}, F_0, \sigma_g, P\right) \quad (4)$$

where $F_0 = \frac{V_0}{\sqrt{g(s-1)d_{50}}}$ is the particle densimetric Froude number and s is the relative density of the particles $\left(\frac{\rho_s}{\rho}\right)$.

AI modelling: a two AI level strategy

Data structure at Level 0

The AIMM strategy is implemented by preparing the dataset and making decisions on modelling structures but these activities are covered at Level 0. The whole purpose is to estimate depth and length of the scouring pit (two dependent variables) in their dimensionless form. According to Equations (3) and (4), dependent variables are described as a function of four independent variables $\left(\frac{y_B}{W}, F_0, \sigma_g, P\right)$. Among the independent parameters, screen porosity (P) is arguably negligible due to limitation in variation of P and interaction between $\frac{y_B}{W}$ and P. Therefore, $\frac{y_B}{W}, F_0, \sigma_g$ are considered as the input dataset and $\frac{D_s}{w}$, $\frac{L_s}{w}$ are considered as the target data for the Level 1 models of SFL and NF. The outputs $\frac{D_s}{w}$, $\frac{L_s}{w}$ from these two models at Level 1 are considered as the input dataset to the Level 2 model, which also shares the same target data. Figure 3 illustrates the structure of the modelling strategy through a flowchart. Notably, 80% of the 25 data obtained by experiments (20 datapoints) were selected randomly and used in the training phase and the remaining 20% of data (five datapoints) were used to test the trained AI models.

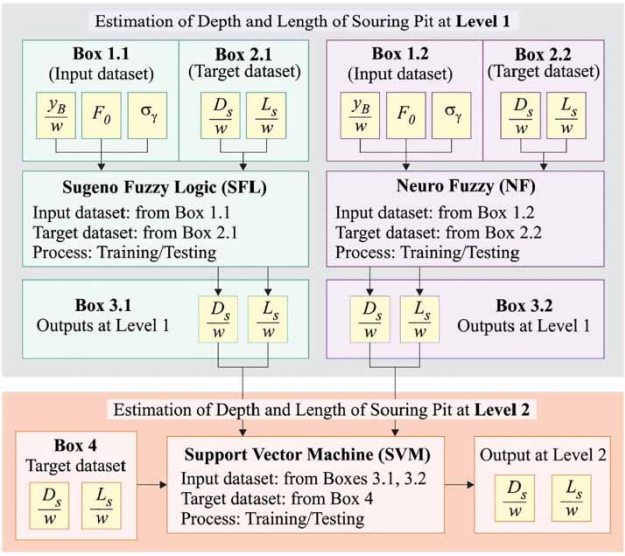

Figure 3 | AI modelling flowchart based on AIMM to estimate depth and length of scouring pit.

AI modelling by Sugeno fuzzy logic (SFL) at Level 1

SFL is now a classic AI technique and the authors' implementation is detailed by Nadiri *et al.* (2018b). The paper employs a clustering technique to identify groupings within the data to automatically derive a rule-base specific to the experimental data and to identify their parameters of membership function (MF), where MF is a key contribution of fuzzy logic. The identification of the grouping in the data leads to an objective representation of systems behaviours within the data through the subtractive clustering (SC) method given by Chiu (1994). SC is parameterised in terms of cluster radius to control the number of clusters and fuzzy rules (Chen & Wang 1999). Identification of the optimum cluster radius is through systematically varying the cluster radius from 0 to 1 until the identification of the optimum values of root mean square errors (RMSE).

The fuzzy if-then rule is expressed in Equation (5) for estimation of depth and length of scouring pit:

$$Rule\ i{:}If \begin{pmatrix} F_0\ belogs\ to\ MF_i \\ \sigma_g\ belongs\ to\ MF_i \\ \frac{y_B}{w}\ belongs\ to\ MF_i \end{pmatrix}, \quad then\left(\frac{D_s}{w}, \frac{L_s}{w} = m_k F_0 + m_i \sigma_g + m_p \frac{y_B}{W}\right) \tag{5}$$

where MF is the membership function, and m_k, m_j and m_p are coefficients. The final output Out_j is the weighted average of all outputs (aggregation) as follows (Sadeghfam *et al.* 2018):

$$Out_j = \frac{\sum_k w_{kj} Out_{kj}}{\sum_k w_{kj}} \tag{6}$$

where w_{kj} is firing strength for rule k and output j, obtained using the 'AND' (minimise) operator.

AI modelling by neuro-fuzzy (NF) at Level 1

NF models integrate fuzzy logic with ANN and, in this way, the derivation of rule-base for fuzzy logic is carried out by ANN through the following steps: (i) input datasets are prepared as above; (ii) SC method and tuned MF related to SFL are used to construct NF. The architecture of NF in this study comprises a five-layer MLP network as follows (Nadiri *et al.* 2018b):

Layer 1: Generate membership function for the input data expressed as:

$$O_i^{\ell=1} = \mu_{ji}(X) \tag{7}$$

where $X = \left\{\frac{y_B}{W}, F_0, \sigma_g\right\}$ and $O_i^{\ell=1}$ is the output of neuron i at layer $\ell = 1$, j is the number of inputs and i is MF index; $\mu_{ji}(X)$ is a fuzzy set associated with neuron i. MF is selected through a trial-and-error procedure and this led to using a generalised Gaussian function.

Layer 2: Calculate firing strength w_i for the i^{th} rule via the multiplication rule:

$$O_i^{\ell=2} = w_i = \mu_{1i}(X)\mu_{2i}(X)\mu_{3i}(X)\mu_{4i}(X)\mu_{5i}(X) \tag{8}$$

Layer 3: Compute the normalised firing strengths for the i^{th} neuron:

$$O_i^{\ell=3} = \overline{w_i} = \frac{w_i}{\sum_i w_i} i = 1, \ldots, 5 \tag{9}$$

Layer 4: Compute the contribution of the i^{th} rule in the model output using first-order SFL:

$$O_i^{\ell=4} = \overline{w_i} GWL_i = \overline{w_i}(m_i GWL + n_i T + p_i R + q_i A + u_i P + c_i) \quad i = 1, \ldots, 5 \tag{10}$$

Layer 5: Calculate the final output as the weighted average of all rule outputs (aggregation):

$$O_i^{\ell=5} = GWL = \sum_i \overline{w_i} GWL_i \tag{11}$$

The NF parameters in Equation (11) and MF parameters are estimated using a hybrid algorithm in this study, which is a combination of the gradient descent and the least-squares method.

Support vector machine (SVM) at Level 2

SVM is a statistical learning technique (Vapnik 1998) and is used here to combine the SFL and NF model outputs. It is a kernel-based learning approach and uses a linear high-dimensional hypothesis space called feature space for implicit kernel functions for mapping, onto which the data are mapped. It is now a widely applied tool, where the implementation of both estimator/predictor problems are similar to neural networks with similar weights and bias. In the formulation of AIMM strategy, input data to the Level 2 SVM model comprise predicted depth and length modelled values of the scouring pit $\left(\frac{D_s}{w}, \frac{L_s}{w}\right)$ at Level 1 using SFL and NF but it shares the target values with the Level 1 models. The regression-type implementation of SVM regresses outputs in terms of inputs, as follows:

$$y(x) = \boldsymbol{w}^T \circ \varphi(\boldsymbol{x}) + b \tag{12}$$

where b is bias values; $\boldsymbol{w}$ is the weight vector; $\varphi(\boldsymbol{x})$ is the non-linear mapping of input data onto a higher-dimensional feature space; the dataset comprises $\{x_i, y_i\}_{i=1}^N$, $x_t \epsilon R^n$, $y_t \epsilon R$, where $\boldsymbol{x}$ is the vector of input data, i.e., the two vectors of $\frac{D_s}{w}$, $\frac{L_s}{w}$ as modelled by SFL and NF; y is the vector of target values in terms of measured data for $\left(\frac{D_s}{w}, \frac{L_s}{w}\right)$; $\boldsymbol{R}^n$ is n-dimensional vector space and $\boldsymbol{R}$ is a one-dimensional array. To identify the parameters inherent in Equation (12), the optimisation problem is formulated by minimising the regular function Equations (13) and (14) as discussed by Suykens *et al.* (2002) in detail. The resulting SVM-LS model for function estimation is as follows:

$$\min R(\boldsymbol{w}, e) = \frac{1}{2}\boldsymbol{w}^T\boldsymbol{w} + \frac{\gamma}{2}\sum_{i=1}^{n} e_i^2 \tag{13}$$

$$y(x) = \sum_{i=1}^{n} \alpha_i K(x_i, \boldsymbol{x}) + b \tag{14}$$

where $K(x_i, \boldsymbol{x})$ is the kernel function; α_i and b are the solutions to the linear system, γ is the positive real constant

to avoid overfitting and noisy data are treated by using a lower γ value. The radial basis function (RBF) is used in this study, which is the most widely used function for the kernel function, expressed as:

$$K(x_i, x_j) = exp\left(\frac{-\|x_i - x_j\|^2}{\sigma^2}\right) \quad (15)$$

where σ is the parameter of kernel function. It is important to select the parameters (γ and σ) with suitable values. This study employs the least-squares (LS) technique through a trial-and-error procedure.

Performance metrics

The performance of AI models at Level 1 and Level 2 are evaluated by RMSE, R^2 and Nash–Sutcliffe coefficient (NSC) in the training and testing phases. For a 'perfect' model with the highest performance, RMSE and R^2 equal to 0 and 1, respectively, but poor performances are reflected in RMSE becoming greater than 0 and R^2 smaller than 1. NSC varies between 1 and $-\infty$, where 1 would correspond to the performance of the 'perfect' model, '0' to very poor performances and NSC ≤ 0 to cases in which the mean of the observed data is a better predictor than the model prediction (Ritter & Muñoz-Carpena 2013).

LABORATORY TESTS TO EXPLAIN SCOURING PROCESSES

As the supercritical flow enters the reach of the stilling basin, different scouring behaviours are observed in Samples 1 to 4; hence, grain sizes have a direct effect on scouring profiles. In smaller grains (Samples 1 and 2 in Figure 2), the following steps are observed. (i) Initially, the supercritical flow jet entering the movable bed is in a parallel state and this provides appropriate conditions for hydraulic jumps (generally in a submerged state) due to the presence of the screen (Figure 4(a)). (ii) Shortly afterwards, scouring is triggered at the bed but grains settle and accumulate forming a scouring ridge at its downstream (Figure 4(b)–4(d)). (iii) As the volume of the scouring pit increases, the height of the scouring pit increases subsequently and as the ridge height exceeds a certain level, it kicks in a steady-state condition such that the scouring ridge and the pit stay stable temporarily (Figure 4(e)–4(h)). (iv) In response to a further rise in ridge height, the depth of scouring increases sharply and the grains accumulate at the bottom of the scouring pit so that the scouring pit is transformed into two separate ridges at the downstream of the scouring pit (Figure 4(i)).

The sharp increase in the scouring depth is attributed to the formation of a clockwise circular flow in response to the resistance forced by the scouring ridge against grains' transport from the scouring pit (see Figure 4(i) and 4(k)). There are reports on the formation of such scouring profile and circular flows, e.g., Balachandar *et al.* (2000); Xie & Lim (2015). These changes in the form of the ridge through circular flows facilitate the transfer of grains to the ridge and its upslope upstream. As the upslope increases and the grains reach the state of their maximum angle of repose, the ridge would suddenly slide and fill the scouring pit (Figure 4(j)). In this state, the circular flow is eliminated. This is a cycle, which would repeat between the states depicted in Figure 4(i) and 4(j). Notably, the bed with larger grain sizes (Samples 3 and 4 in Figure 2) do not show such a cycle due to the increased resistance of grains against scouring (see Figure 4(l)).

RESULTS

Analysis of the profiles

Figure 5 displays scouring profiles in various time intervals for Sample Beds 1 to 4 for P40 and P50 screens, in which the x-axis displays longitudinal dimensionless coordinates (x/x_s), where x is the longitudinal coordinate and x_s is the distance between screen location and the sluice gate. The y-axis introduces the level of bed deformation using a dimensionless state number, (y/w). These are collectively indicative of more scouring depth in the P40 screen than the P50 screen. This is explained by the fact that the P40 screen has less porosity than that of P50, which results in further scour depths upstream of the screen. Previous

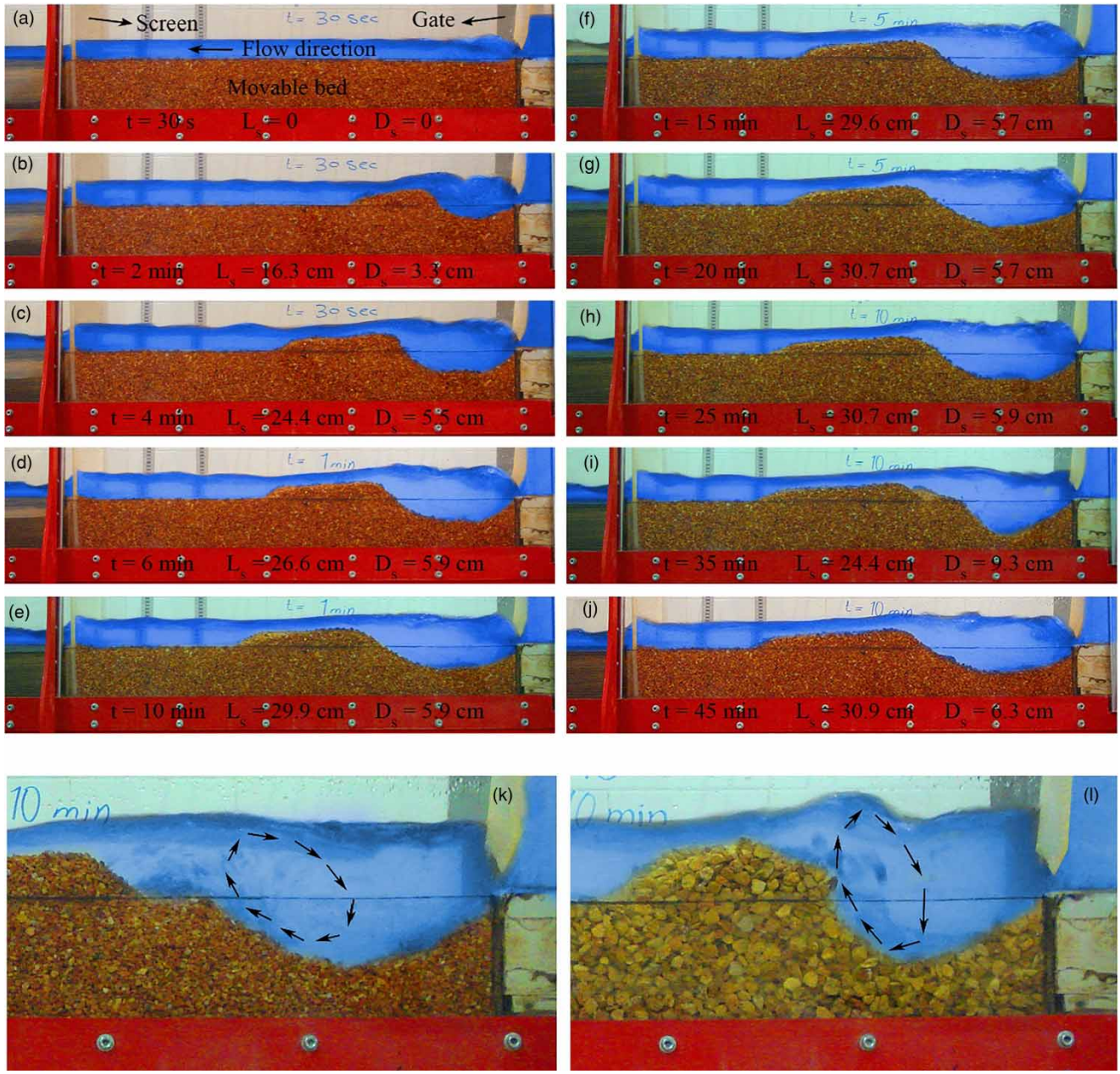

Figure 4 | (a)–(j) Chronological scouring changes (Sample 1, P50 screen) in $Fr_A = 7.5$; (k) and (l) increase in scouring depth due to circular flow in the upstream of ridge near the scouring pit: (k) Sample bed 1, P50 screen, $Fr_A = 7.5$ and $Fr_0 = 8.68$; (l) Sample bed 3, P40 screen, $Fr_A = 7.5$ and $Fr_0 = 5.43$.

studies also reveal that as the tailwater increases scouring depth in sand grains increase (Xie & Lim 2015).

Existence of the scouring cycles in Figure 4 is also depicted in Figure 5(b), for which the establishment of the scouring profile took 44 minutes to form two separate ridges but in the 45th minute, the accumulated grains returned to the scouring pit and transformed the regular scouring profile again. For smaller grains (Samples 1 and 2), the scouring ridge moves toward downstream and the form of the scouring ridge expands into a flatter state from its parabolic shape (see Figures 5(a)–5(c) and 6(d)). As the flow depth over the scouring ridge decreases, the flow

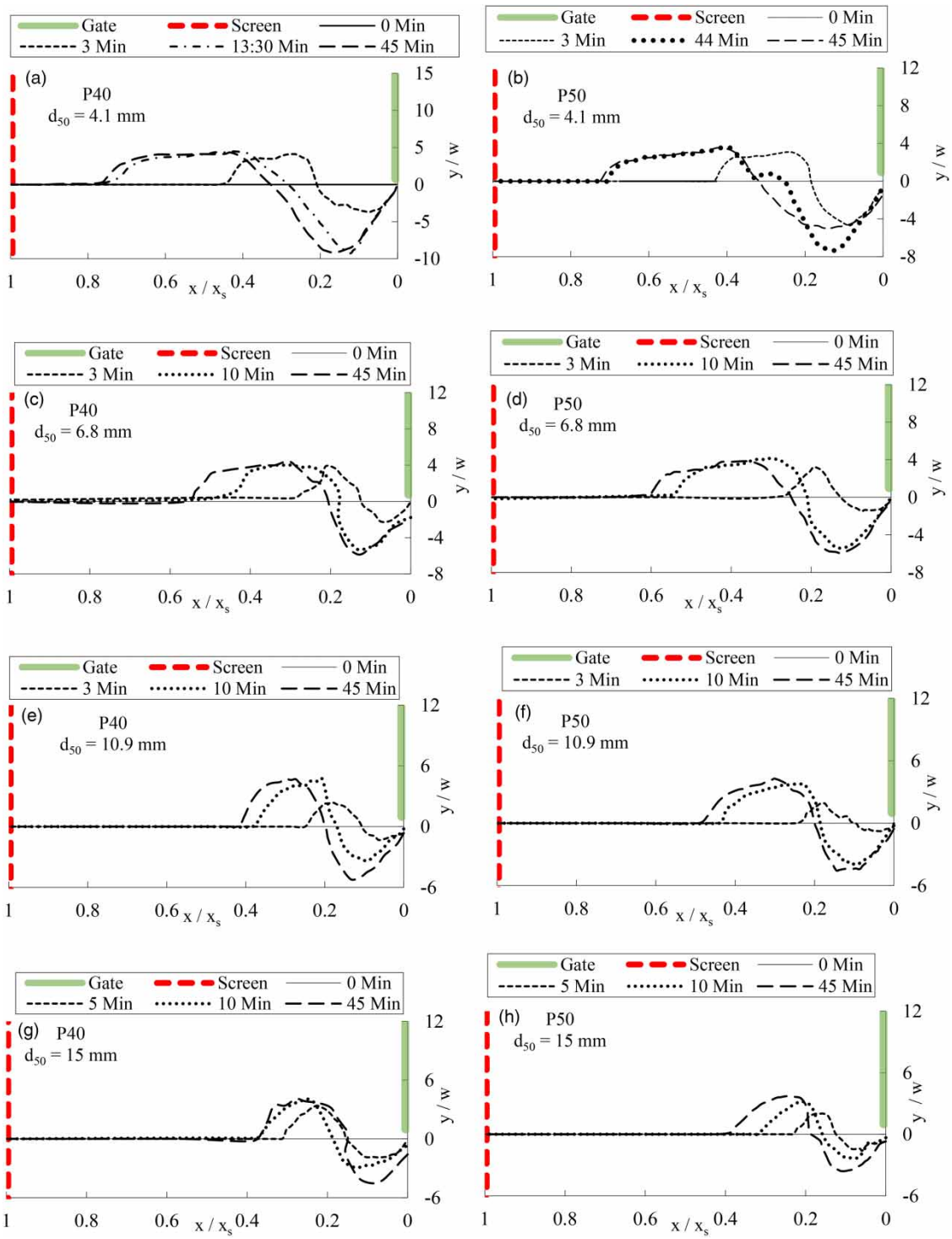

Figure 5 | Scouring profiles at different discharge intervals $Fr_A = 7.5$ (Samples 1 to 4).

moves at a faster rate and, therefore, its grain transport rate increases. As a result, the scouring ridge is transferred towards downstream over a further length.

Scouring profiles are investigated for larger grain samples (Samples 3 and 4). It is observed that the scouring ridge slope is larger than those with smaller grains (Samples

1 and 2) and larger grains form steeper scouring pits and ridges as their angles of repose is larger (Figure 5(e)–5(h)).

An insight into the behaviour of scouring dimensions

According to Equations (3) and (4), scouring dimensions are expressed as a function of four dimensionless parameters, which comprise: (i) the particle densimetric Froude number (Fr_0); (ii) standard deviation of particles (σ_g); (iii) dimensionless depth on screen upstream at section B $\left(\frac{y_B}{W}\right)$; (iv) screen porosity ($P$). This section discusses the behaviour of scouring dimension in response to these dimensionless parameters.

Effects of flow depth on screen upstream (section B)

Water depth at the upstream of the screen (y_B) changes according to the inflow condition (Froude number of supercritical flow), screen porosity and the size of bed materials. Previous studies demonstrate the effect of tailwater on the scouring pit so that the maximum scouring depth increases as the depth of the tailwater increases (Xie & Lim 2015). Likewise, in the present study, the performance of water depth in the upstream of the screen (y_B) is like the effect of the tailwater forming scouring pits by supercritical flow jets. Figure 6(a1) and 6(a2) represent the changes in dimensionless parameter of maximum depth and maximum length

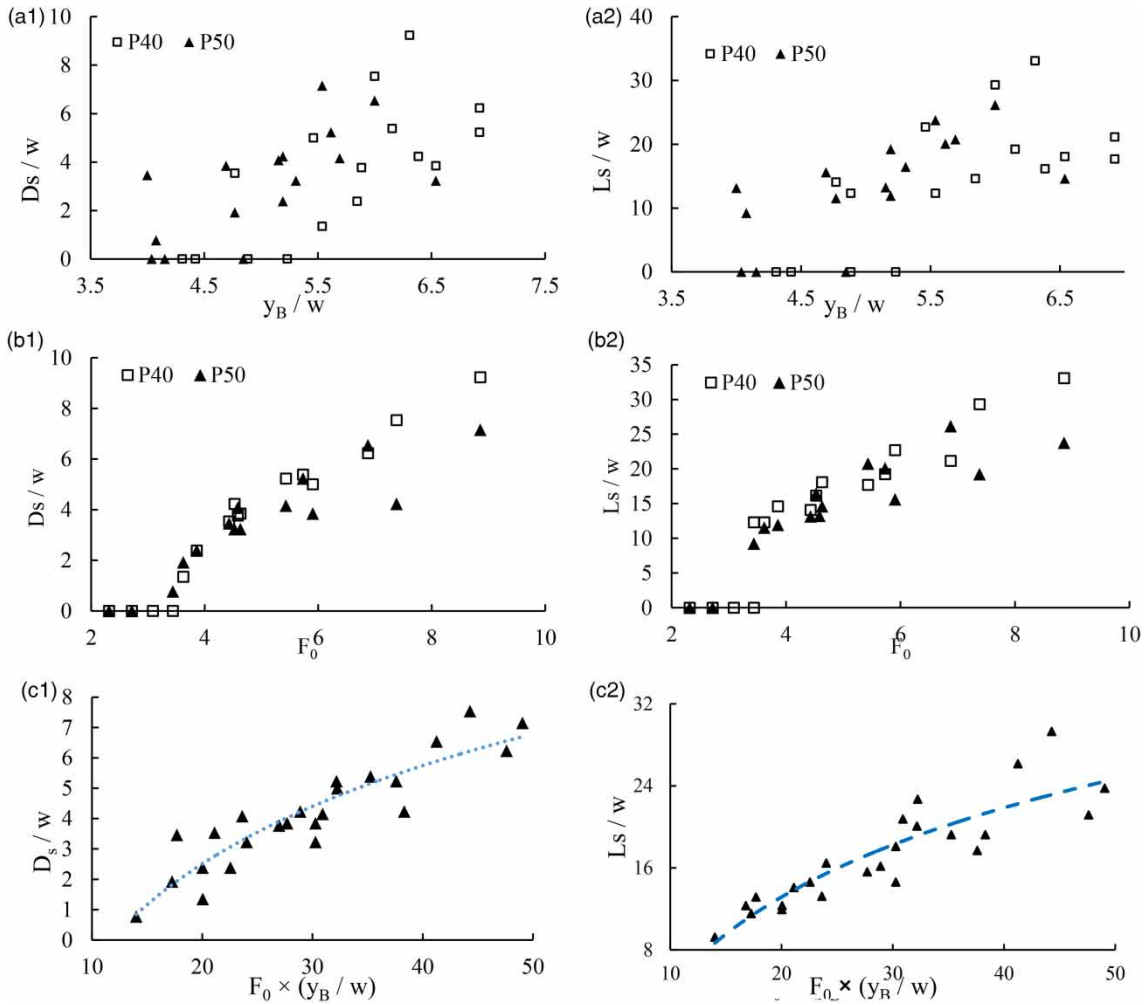

Figure 6 | Relationship between maximum scouring dimensions with: (a1) and (a2) the effect of flow depth (y_B/w) in upstream of the screen; (b1) and (b2) Froude number (F_0); (c1) and (c2) the product of particle densimetric Froude number and upstream flow depth at the screen.

of scouring proportional to dimensionless parameter of y_B/w for P40 and P50 screens.

As shown in Figure 6(a1) and 6(a2), an increase in flow depth at the upstream of the screen is studied, which shows that it affects the maximum depth and length of the scouring pit. The figure also shows the dimensions of the scouring pit (length and depth), in which scours for the P40 screen are greater than the ones for the P50 screen. Average values of this difference for their maximum depth and length are calculated to be 11% and 14% greater, respectively. As the porosity of the P50 screen is greater than the P40 one, flow depth and therefore the scouring depth in the upstream of the P40 screen is greater than that of the P50 screen under equal conditions of supercritical Froude numbers. It should be noted that scouring depth depends not only on flow depth in the upstream screen but also on the particle densimetric Froude number. Thus, in some cases, the increase in tailwater decreases scouring depth due to the effect of the particle densimetric Froude number.

Effect of particle densimetric Froude number

The particle densimetric Froude number is one of the dimensionless parameters as expressed by Equation (3), which has a direct relationship with the velocity of the input jet and a reverse relationship with the square of the median of grain size. As the velocity of the input jet increases, forces imposed by fluid increase on particles and, this in turn, increases the scouring rate. Besides, a decrease in the size of grains decreases resistant forces against the force imposed by fluid and this sets up grain movements by fluids. Experimental tests show (see Figure 6(b1) and 6(b2)) both particle densimetric Froude number and the dimensions of the scouring pit would reach their maximum when the Froude number of supercritical flow jets would reach their maximum ($Fr_A = 7.5$) and this would correspond to small bed grains (Sample 1). Considering the range of changes in the median of grain diameters and the velocity of the input jet, it was observed that the effect of grain size was less than those of the jet velocity changes. Thus, minimum scouring was affected by lower velocity and larger grain size with the first and second priorities, respectively, as contributing factors.

Figure 6(b1) and 6(b2) illustrate the changes in maximum depth and length of scouring proportional to particle densimetric Froude number for P40 and P50 screens. The figure shows that an increase in particle densimetric Froude number increases maximum depth and length of scouring. This increase in scouring could be attributed to the decrease in size of the particles, increase in flow velocity and/or their joint effect. Considering the fact that conditions of the input jet, grading of bed material and the particle densimetric Froude number in P40 and P50 screens are equal, the difference in maximum scouring depth for P40 and P50 screens could be the result of differences in the flow depth in the screen upstream (y_B). Furthermore, as can be seen in Figure 6(b1) and 6(b2), scouring is not created for particle densimetric Froude numbers below 3.5.

Effects of particle densimetric Froude number and upstream depth on the screen

The joint effect of both particle densimetric Froude number and flow depth at the upstream of the screen is investigated on the scouring dimensions using the dimensionless parameter of $F_0\frac{y_B}{w}$. Figure 6(c1) and 6(c2) depict variation of $F_0\frac{y_B}{w}$ versus dimensionless parameter of maximum depth and length of scouring pit along with the trend curve obtained by fitting of logarithmic equation.

SVM running AIMM to predict dimensions of scouring pits

The functional relationships in the pit dimensions is yet to be expressed in mathematical terms. The functions may be identified by expressing them as regression equations. However, AI provides a far neater approach and hence the results of using the AIMM strategy is presented below, which fits SFL and NF models at Level 1 and SVM at Level 2. The SFL model uses the data clustering method and the paper employs the RMSE criterion to identify the cluster radii by a systematic trial-and-error procedure, and hence the identified cluster radii is 0.85. SFL uses generalised Gaussian function to express membership functions for the input dataset. The NF model incorporated the same cluster through the SC method for input and target datasets as those for SFL. The model parameters were

Table 2 | Results from goodness-of-fit test for AI models at Level 1 and Level 2

	RMSE			R^2			NSC		
	Total	Training	Testing	Total	Training	Testing	Total	Training	Testing
SFL at Level 1	3.41	1.14	7.3	0.930	0.990	0.869	0.909	0.990	0.348
NF at Level 1	2.8	0.81	6.07	0.940	0.995	0.913	0.938	0.995	0.540
SVM at Level 2 (AIMM)	1.71	0.38	3.74	0.980	0.999	0.937	0.997	0.999	0.823
Percentage (%) of improvement (SFL-SVM)	99	200	95	5	1	7	9	1	58

The SVM parameters are: $\gamma = 2$, $\sigma = 0.1$.

estimated through the combination of the backpropagation gradient descent method (Jang *et al.* 1997) with the least-squares method (see Equation (10)) and the Gaussian membership functions. At Level 2, SVM used the outputs from SFL and NF as input data.

Table 2 presents the performance metrics for SFL, NF, SVM models and Figure 7 depicts the scatter diagram and their residual errors for SFL, NF, SVM for both predictive models of $\frac{D_s}{w}$ and $\frac{L_s}{w}$. These results provide evidence that the modelling strategy at Level 1 produces results fit-for-purpose and at Level 2, improvements on RMSE are remarkable, on R^2 are significant, on NSC reveal that SVM at Level 2 is more robust and the reduction in the scatter is evident.

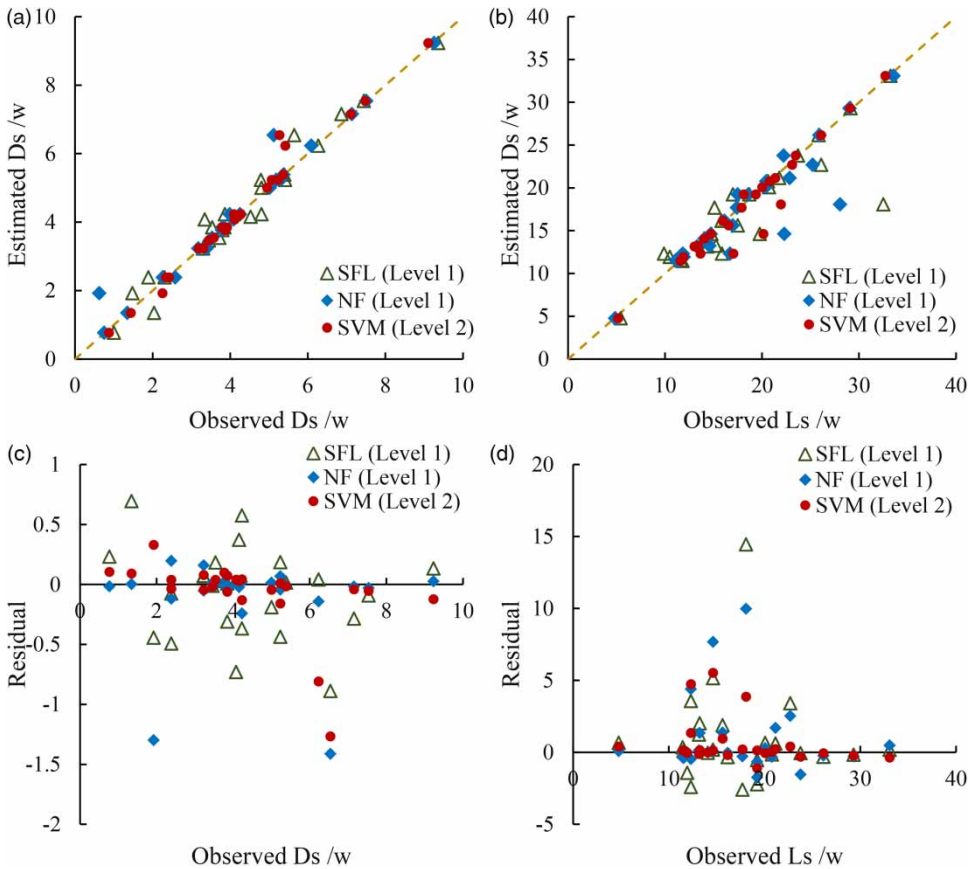

Figure 7 | Scatter diagram and residual error for dimensionless parameters of: (a) and (c) depth; (b) and (d) length of pit.

DISCUSSION

Screens, widely used maintenance components in watercourses, operate by-and-large under subcritical flows, where they cause some affluxes. However, their performances under supercritical flows for energy dissipation at downstream of small hydraulic structures is a recent realisation. As screens are eco-friendly structures and widely used maintenance measures, their provision for energy dissipation is also attractive and the paper presents laboratory results to provide evidence that their provision in moveable beds is also feasible. However, the investigation for producing design guidelines are not yet in the remit of this work, as this is the ultimate goal for a future work.

To produce guidelines, attention needs to be paid to inherent problems associated with shortfalls of screens, as they are liable to give rise to blockage problems by debris flows and the weaving of leaves, tree branches and twigs to screens. In developed countries, they are regularly maintained including off-schedule maintenances after major flooding incidents. Robust designs should consider maintenance scenarios including a blockage and their impacts on scouring, as well as the flooding of local areas under supercritical flow regimes. Also, the performance of prototypes in natural watercourses should be investigated for a better understanding.

This study takes a step towards understanding scour patterns and their hydraulics behaviour induced by screens. Following the proof-of-concept reported by the paper, the future phases of this research will focus on investigating a wide range of movable bed grading, screen porosities and supercritical Froude numbers ranges (although the reported results comply with the range of Froude number recommended by the United States Bureau of Reclamation (USBR) IV for stilling basins). Also, the future investigations will consider the scouring of finer sediments as in natural rivers, as the remit of this work is on coarser granular materials.

CONCLUSION

Laboratory studies of scouring of supercritical flows against screens are presented. In spite of past thriving studies on energy dissipation through screens, an investigation on scouring in stilling basins under supercritical flows over moveable beds is yet to become topical. The paper reports on a set of data including: Froude number of supercritical flow for the movable bed of the stilling basin (in the range of 3.5 to 8); the particle densimetric Froude number (in the range of 2 to 10 5) samples of gravel beds (median diameter in the range of 1.4 to 24 mm), where their grain size contributes to stabilising the channel bed. As well, experiments were conducted on two types of screen with porosities of 40 and 50% with a single arrangement.

The problem was conceptualised in terms of four variables to express scouring pit dimension: depth and length of pit. Experimental data were produced to learn the hydraulic behaviour of the formation of the pits under different hydraulic and gravel parameters. A modelling strategy was formed to fit AI models to the data to provide predictive tools. This comprised AI models at two levels: at Level 1 SFL and NF provided fit-for-purpose results and these were to SVM at Level 2. The result reveals that the strategy gives a remarkable improvement of models at Level 1. The paper explains the scouring process and shows the pit dimensions can be predicted with reasonable accuracy. Further works are required to provide design guidance.

REFERENCES

Balachandar, R., Kells, J. A. & Thiessen, R. J. 2000 The effect of tailwater depth on the dynamics of local scour. *Can. J. Civil Eng.* **27** (1), 138–150.

Bozkuş, Z. & Aslankara, V. 2008 Tailwater effect on the energy dissipation through screens. In: *Proceedings of the 8th International Congress on Advances in Civil Engineering*. Eastern Mediterranean University, Famagusta, North Cyprus.

Bozkuş, Z., Çakır, P., Ger, M. & Ozeren, Y. 2004 Energy dissipation through screens. In: *Proceedings of the 2004 World Water and Environmental Resources Congress*, Salt Lake City, UT, USA. ASCE, pp. 1–8.

Bozkuş, Z., Balkış, G. & Ger, M. 2005 Effect of inclination of screens on energy dissipation downstream of small hydraulic structures. In: *Proceedings of the 17th Canadian Hydrotechnical Conference*, Edmonton, Alberta, Canada, pp. 881–890.

Bozkuş, Z., Güngör, E. & Ger, M. 2006 Energy dissipation by triangular screens. In: *Proceedings of the Seventh*

International Congress on Advances in Civil Engineering. Yıldız Technical University, Istanbul, Turkey.

Bozkuş, Z., Çakır, P. & Ger, M. 2007 Energy dissipation by vertically placed screens. *Can. J. Civil Eng.* **34** (4), 557–564.

Çakır, P. 2003 *Experimental Investigation of Energy Dissipation Through Screens*. MSc thesis, Department of Civil Engineering, Middle East Technical University, Ankara, Turkey.

Castillo, L. G. & Carrillo, J. M. 2017 Comparison of methods to estimate the scour downstream of a ski jump. *Int. J. Multiph. Flow* **92**, 171–180.

Chen, M. S. & Wang, S. W. 1999 Fuzzy clustering analysis for optimizing fuzzy membership functions. *Fuzzy Sets Syst.* **103** (2), 239–254.

Chiu, S. L. 1994 Fuzzy model identification based on cluster estimation. *J. Intell. Fuzzy Syst.* **2** (3), 267–278.

Choi, S. U., Choi, B. & Choi, S. 2015 Improving predictions made by ANN model using data quality assessment: an application to local scour around bridge piers. *J. Hydroinform.* **17** (6), 977–989.

Daneshfaraz, R., Sadeghfam, S. & Ghahramanzadeh, A. 2017 Three-dimensional numerical investigation of flow through screens as energy dissipators. *Can. J. Civ. Eng.* **44** (10), 850–859.

Houichi, L., Dechemi, N., Heddam, S. & Achour, B. 2013 An evaluation of ANN methods for estimating the lengths of hydraulic jumps in U-shaped channel. *J. Hydroinform.* **15** (1), 147–154.

Jang, J. S. R., Sun, C. T. & Mizutani, E. 1997 Neuro-fuzzy and soft computing – a computational approach to learning and machine intelligence (Book Review). *IEEE Trans. Autom. Contr.* **42** (10), 1482–1484.

Nadiri, A. A., Gharekhani, M., Khatibi, R., Sadeghfam, S. & Moghaddam, A. A. 2017 Groundwater vulnerability indices conditioned by supervised intelligence committee machine (SICM). *Sci. Total Environ.* **574**, 691–706.

Nadiri, A. A., Gharekhani, M. & Khatibi, R. 2018a Mapping aquifer vulnerability indices using artificial intelligence-running multiple frameworks (AIMF) with supervised and unsupervised learning. *Water Resour. Manage.* **32** (9), 3023–3040.

Nadiri, A. A., Sedghi, Z., Khatibi, R. & Sadeghfam, S. 2018b Mapping specific vulnerability of multiple confined and unconfined aquifers by using artificial intelligence to learn from multiple DRASTIC frameworks. *J. Environ. Manage.* **227**, 415–428.

Rajaratnam, N. & Hurtig, K. I. 2000 Screen-type energy dissipator for hydraulic structures. *J. Hydraul. Eng.* **126** (4), 310–312.

Ritter, A. & Muñoz-Carpena, R. 2013 Performance evaluation of hydrological models: statistical significance for reducing subjectivity in goodness-of-fit assessments. *J. Hydrol.* **480**, 33–45.

Roushangar, K. & Ghasempour, R. 2019 Evaluation of the impact of channel geometry and rough elements arrangement in hydraulic jump energy dissipation via SVM. *J. Hydroinform.* **21** (1), 92–103.

Roushangar, K., Akhgar, S., Erfan, A. & Shiri, J. 2016 Modeling scour depth downstream of grade-control structures using data driven and empirical approaches. *J. Hydroinform.* **18** (6), 946–960.

Roushangar, K., Khowr, A. F. & Saneie, M. 2019 Influential parameters on submerged discharge capacity of converging ogee spillways based on experimental study and machine learning-based modeling. *J. Hydroinform.* **21**, 474–492.

Sadeghfam, S., Akhtari, A. A., Daneshfaraz, R. & Tayfur, G. 2014 Experimental investigation of screens as energy dissipaters in submerged hydraulic jump. *Turk. J. Eng. Env. Sci.* **38** (2), 126–138.

Sadeghfam, S., Ehsanitabar, A., Khatibi, R. & Daneshfaraz, R. 2018 Investigating 'risk' of groundwater drought occurrences by using reliability analysis. *Ecol. Indicators* **94**, 170–184.

Sahraei, S., Alizadeh, M. R., Talebbeydokhti, N. & Dehghani, M. 2018 Bed material load estimation in channels using machine learning and meta-heuristic methods. *J. Hydroinform.* **20** (1), 100–116.

Suykens, J. A., Van Gestel, T. & De Brabanter, J. 2002 *Least Squares Support Vector Machines*. World Scientific, Singapore.

Toth, E. & Brandimarte, L. 2011 Prediction of local scour depth at bridge piers under clear-water and live-bed conditions: comparison of literature formulae and artificial neural networks. *J. Hydroinform.* **13** (4), 812–824.

Uyumaz, A., Danandeh Mehr, A., Kahya, E. & Erdem, H. 2014 Rectangular side weirs discharge coefficient estimation in circular channels using linear genetic programming approach. *J. Hydroinform.* **16** (6), 1318–1330.

Vapnik, V. N. 1998 An overview of statistical learning theory. *IEEE Trans. Neural Netw.* **10**, 988–999.

Xie, C. & Lim, S. Y. 2015 Effects of jet flipping on local scour downstream of a sluice gate. *J. Hydraul. Eng.* **141** (4), 4014088.

First received 7 April 2019; accepted in revised form 27 June 2019. Available online 24 July 2019